ACS APPLIED NANO MATERIALS
Cite This: ACS Appl. Nano Mater. 2018, 1, 3098−3104
Letter
www.acsanm.org

Fabrication of Cellulose Nanocrystal Films through Differential Evaporation for Patterned Coatings

Andy Tran,[†] Wadood Y. Hamad,[‡] and Mark J. MacLachlan*[,†]

[†]Department of Chemistry, University of British Columbia, 2036 Main Mall, Vancouver, British Columbia V6T 1Z1, Canada
[‡]FPInnovations, 2665 East Mall, Vancouver, British Columbia V6T 1Z4, Canada

Supporting Information

ABSTRACT: Cellulose nanocrystal (CNC) films were patterned by controlling the evaporation time of CNC suspensions. It is known that the evaporation time, and by extension the self-assembly process, influences the optical properties of the resulting films, but the patterning of CNC films has not been extensively investigated. Here, we demonstrate an easy new approach to the patterning of CNC films by varying the evaporation time at different regions of a drying CNC suspension, which produce films with drastically different optical properties. Furthermore, the application of cellulose acetate masks to restrict evaporation can also be used to develop patterned CNC films.

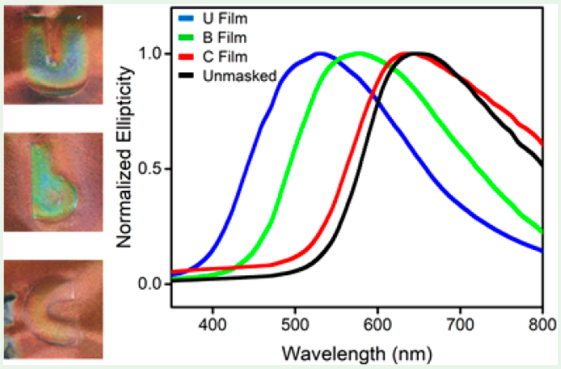

KEYWORDS: *cellulose nanocrystals, self-assembly, patterns, evaporation, optical properties*

INTRODUCTION

Cellulose is the most abundant biopolymer on earth, found in plant cell walls, wood, tunicates, and bacteria.[1] Cellulosic sources treated with sulfuric acid can undergo acid-catalyzed hydrolysis, leaving behind crystalline spindle-shaped particles with typical dimensions of 5−30 nm × 100−500 nm.[2−5] These particles, called cellulose nanocrystals (CNCs), are attractive candidates for materials development and fabrication owing to their inexpensive sourcing from wood or cotton and their fascinating optical and mechanical properties.[6−9] CNCs have been explored for various applications including material printing, tissue engineering, and optical filters, among others.[1,10−13] Furthermore, many studies have been conducted to further our understanding of CNCs, from a macroscopic perspective, in the development of solid film materials all the way down to the microscopic self-assembly process.[6,14,15]

The use of sulfuric acid mediated hydrolysis leaves negatively charged sulfate groups on the CNC surface, which enables them to form a stable colloidal dispersion in water.[16,17] When concentrated in water, a stable colloidal dispersion of CNCs adopts a chiral nematic lyotropic liquid crystal with a left-handed helical orientation.[18] CNCs assemble into this long-range liquid-crystalline phase through short-range-ordered structures called tactoids, and the chiral nematic structure can be preserved in solid films upon complete evaporation of the water.[6,19] The optical properties of CNCs arise from the helical structure according to eq 1.[20] In particular, the reflectance wavelength λ at angle θ depends on the refractive index n and helical pitch P. The dependence of angle θ with respect to the surface of the film gives CNC films brilliant iridescence, similar to many examples found in nature.[21−24]

$$\lambda = nP \sin \theta \quad (1)$$

The optical properties imparted by the helical pitch have been reported by many groups and are influenced by the additives, temperature, humidity, evaporation, magnetic fields, electric fields, substrate variations, and ionic strength.[25−32] Further studies looked at the self-assembly process in detail over various stages, including (a) phase separation, (b) gel vitrification, and (c) film formation.[27] In our earlier work, we proposed an intermediate stage of self-assembly, called tactoid annealing, that also influences the chiral nematic order and the helical pitch of the resulting CNC films.[33] This finding revealed even more complexities when dealing with CNC systems. There have been few studies detailing the production of photonic patterns in CNC films. Beck et al. reported the use of heat to produce areas of different thicknesses, which resulted in patterned CNC films.[34] However, patterned CNC films without the use of additives or temperature variations are particularly interesting for their improved optical quality and control. Patterned CNC films with structural variations with spatial control open up potential applications in optical filters and sensors.

Here, we report a simple method for controlling the optical properties in CNC films, and we use the new method to

Received: June 6, 2018
Accepted: June 11, 2018
Published: June 18, 2018

DOI: 10.1021/acsanm.8b00947
ACS Appl. Nano Mater. 2018, 1, 3098−3104

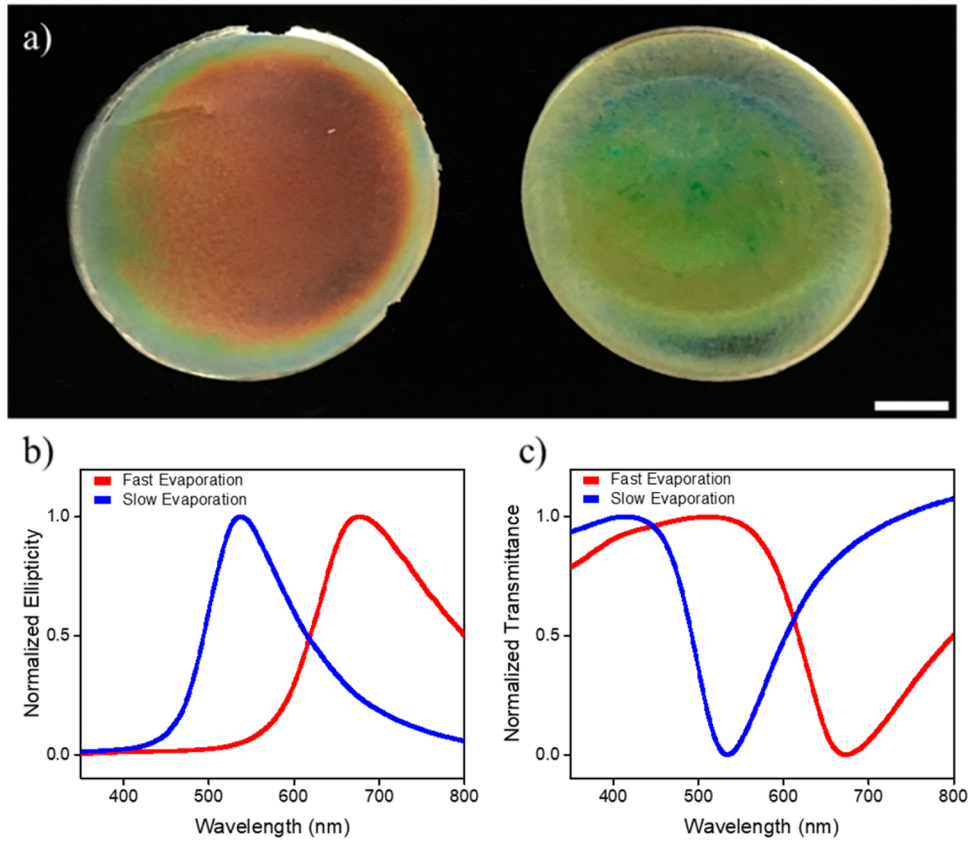

Figure 1. Influence of the evaporation time on the optical properties of CNC films. (a) CNC films prepared by evaporation over 1 day (left) or 10 days (right). The scale bar represents 1 cm. (b) CD and (c) UV−vis spectra of CNC films.

Scheme 1. Visual Representation of a Differential Evaporation Experiment[a]

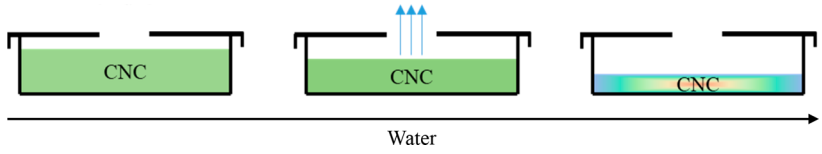

[a]A polystyrene Petri dish containing a CNC suspension is covered by a lid with a 1 cm circular opening at the center. CNC films are formed upon complete evaporation of water.

produce patterned CNC films. By applying differential evaporation to regions of the same CNC film, we are able to vary the self-assembly process and produce regions that have different optical properties. In doing so, we demonstrate that CNC films can be easily patterned without the use of additives or harsh conditions. We further demonstrate that the localized restriction of evaporation with pieces of cellulose acetate allows for the incorporation of patterned optical features in the film. These results advance our understanding of the self-assembly process of CNC films and will help to bridge the gap toward the development of CNC materials of the future.

RESULTS AND DISCUSSION

Effect of Evaporation on CNC Film Formation. From previous work, the evaporation time of a CNC suspension has a significant influence on the optical properties of the resulting CNC films.[25] To demonstrate, CNC films were prepared from a CNC suspension with two evaporation times, either 1 day or 10 days. CNC suspensions evaporated under ambient conditions in 1 day produced red films, whereas longer evaporation times resulted in green films (Figure 1a).

Both circular dichroism (CD) and UV−vis spectroscopy of the films showed that longer evaporation times lead to blue-shifted reflection wavelengths (Figure 1b,c). The blue shift observed in the CD spectra of films prepared for longer evaporation times suggests a difference in the microstructures, specifically the helical pitch. Differential evaporation gave films with different optical properties, which can be useful for the development of patterned CNC films.

Patterning of CNC Films by Differential Evaporation. By a simple change in the evaporation time of a drying CNC suspension, it is possible to significantly change the optical properties of films without the use of additives, temperature gradients, or other external influences. We can take advantage of this evaporation dependence to develop films with various optical patterns. To investigate this, a simple evaporation experiment was conducted to test the feasibility of using evaporation to pattern CNC films from an initially free-flowing CNC suspension. A Petri dish containing the aqueous CNC

DOI: 10.1021/acsanm.8b00947
ACS Appl. Nano Mater. 2018, 1, 3098−3104

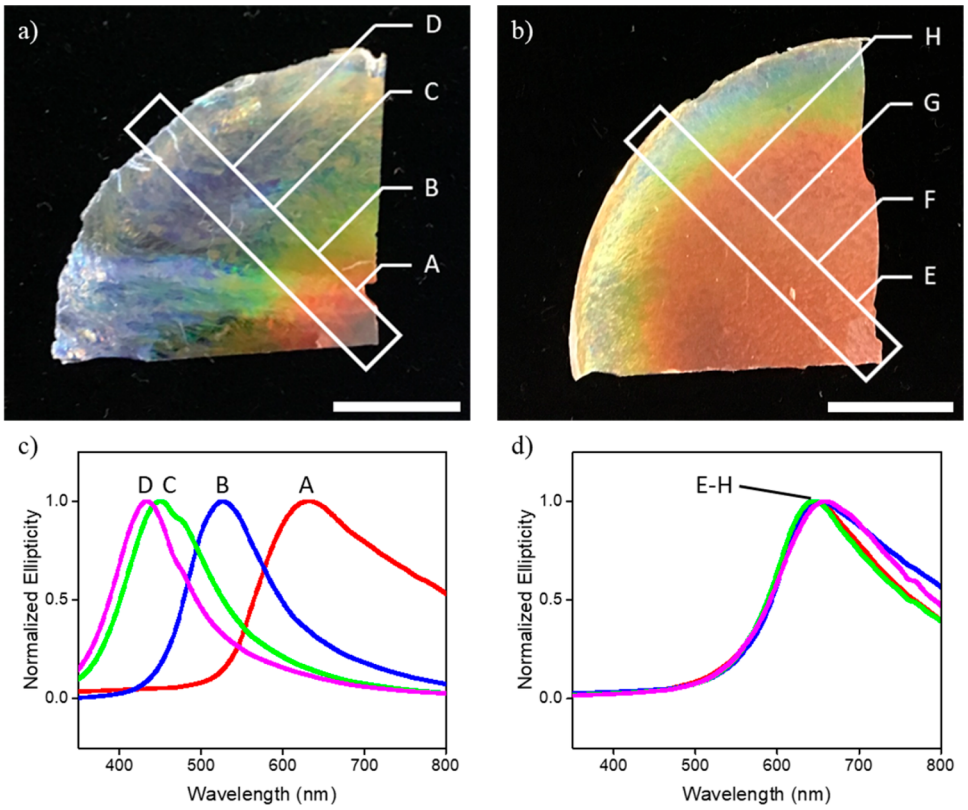

Figure 2. Differential evaporation of a CNC suspension leading to a film with an optical gradient. (a) CNC film with a gradient pattern that blue-shifts, moving away from the center. The regions are marked as A–D; each region is separated by 5 mm. (b) Control CNC film. The regions are marked as E–H; each region is separated by 5 mm. (c) CD spectra collected at regions labeled as A–D for the CNC film prepared with an optical gradient. (d) CD spectra collected at regions labeled as E–H for the control CNC film. The scale bars represents 1 cm.

suspension (4.2 wt %) was capped with a lid containing a 1 cm circular opening at the center (Scheme 1).

We hypothesized that the CNC suspension directly beneath the opening would evaporate more quickly than the rest of the suspension, resulting in a CNC film with a red center and blue color away from the center. Indeed, as shown in Figure 2a, the resulting CNC film displays an optical gradient, with a red center and a gradual shift toward blue heading away from the center. Compared to the control film, the gradient only appears near the edge of the film, which can be attributed to rapid evaporation in the final stages of drying. The CNC film was characterized by CD spectroscopy at various locations, measured at intervals of 5 mm, starting from the center (Figure 2c).

By a simple change of the evaporation rate across different regions of the same film, an optical gradient can be produced. The gradient can be tuned by changing the size of the opening, which changes the evaporation profile, or by changing the height at which the opening rests above the suspension. We noticed that the reflection maximum of the center of the film appears to be outside the visible spectrum, approaching IR. We hypothesize that the region directly below the opening is chaotic during evaporation, which influences the structure in the final CNC film. Harris et al. described the use of evaporative lithography to investigate the lateral transport of colloidal microspheres under the influence of a mask.[35] Lateral transport in our system is likely happening, but we find that film thicknesses are consistent throughout the film. We cannot rule out contributions to the optical properties due to small differences in thickness, but we believe the major contributor is a difference in structure (Figure S1), primarily the pitch of the structure. These differences are likely responsible for the optical gradient observed. Nevertheless, this experiment demonstrates that we can take advantage of differential evaporation to produce patterned films.

Patterning of CNC Films with Masks. We initially attempted to pattern CNC films with different shapes at the opening, but the resolution of the resulting pattern was low and the evaporation profile at the center and edges resulted in films with defects (Figure S1). The patterns were improved by lowering the opening to slightly less than 5 mm from the CNC suspension. However, we hypothesized that the simple placement of a mask on the drying CNC suspension might provide more contrast between two differentially evaporating regions.

In order to apply a mask directly to the surface of the aqueous CNC suspension, we needed to find a material that was insoluble in water and would not itself affect the final optical properties of the CNC film. After testing several possible materials, we selected colorless, transparent masks made of cellulose acetate. Films of CNCs cast on both polystyrene and cellulose acetate have almost identical optical properties (Figure S2), indicating that the cellulose acetate itself does not significantly affect the pitch of the CNC films. We predicted that two distinct regions would arise, one under the mask, where evaporation is slow, and another outside of the mask, where evaporation can occur faster; this would lead to the formation of a patterned CNC film. To confirm this, we cast a CNC suspension and immediately placed a 1 cm circular cellulose acetate mask on top of the suspension, in the center,

DOI: 10.1021/acsanm.8b00947
ACS Appl. Nano Mater. 2018, 1, 3098–3104

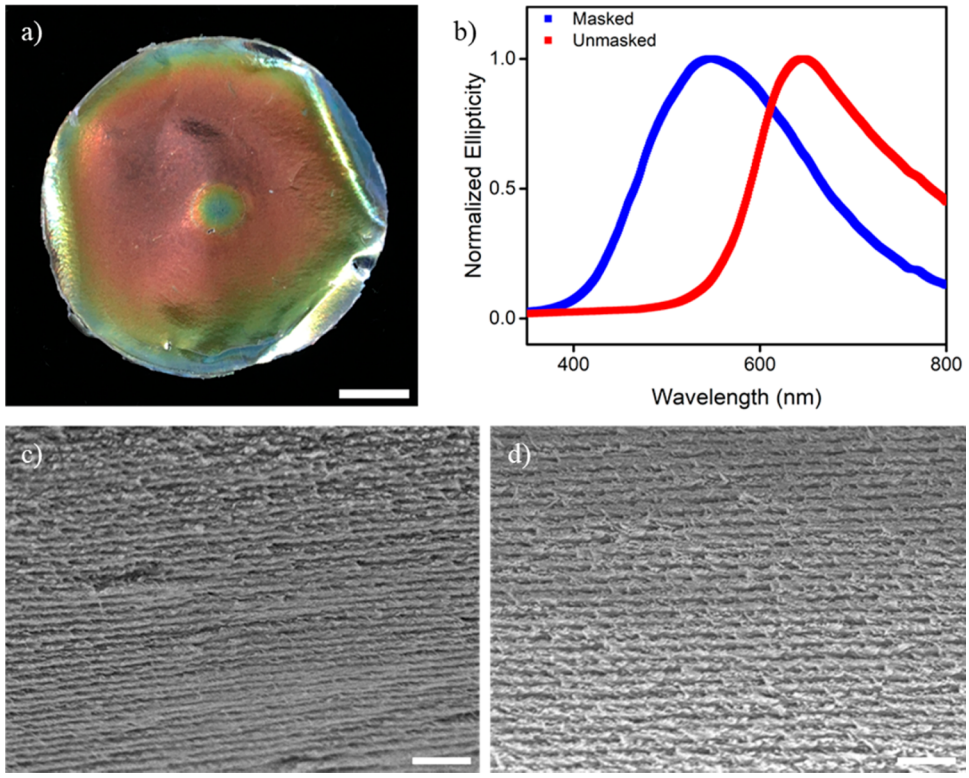

Figure 3. Patterned CNC film using a cellulose acetate mask. The mask was immediately placed on top of a drying CNC suspension and left undisturbed until film formation, upon which the mask was removed. (a) Photograph of the patterned CNC film. (b) CD spectra of two regions, masked and unmasked. Cross-sectional SEM images of the (c) masked and (d) unmasked regions. The scale bars represent (a) 1 cm and (c and d) 1 μm.

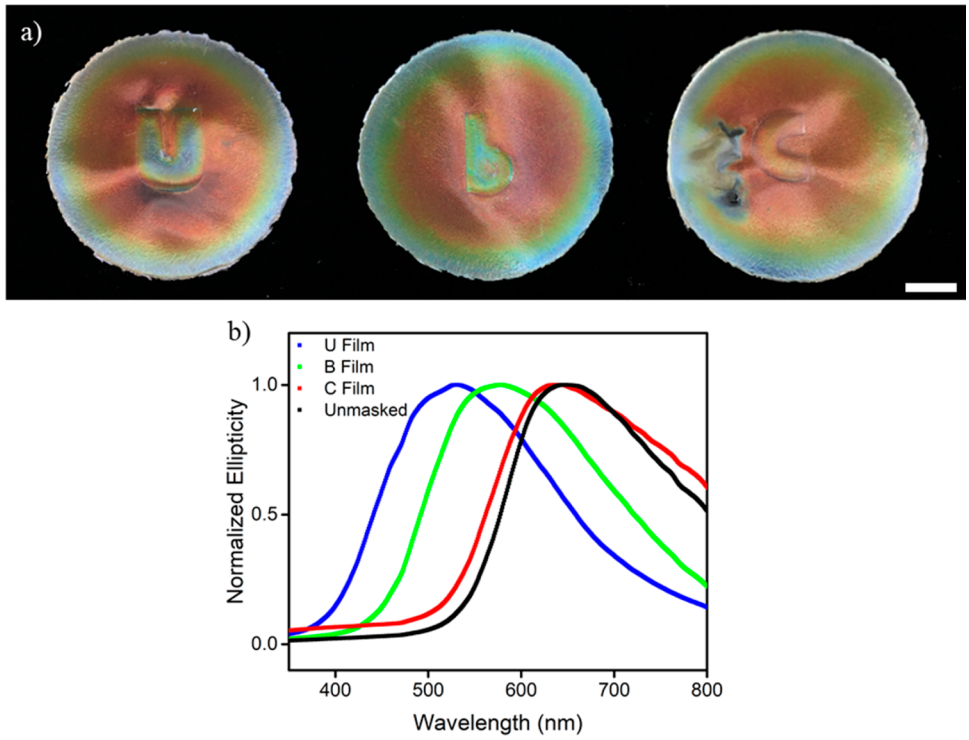

Figure 4. Patterning of CNC films with cellulose acetate masks. (a) Photograph of patterned CNC films for which masks were placed 0 h (left), 6 h (middle), or 9 h (right) after casting the CNC suspensions. The scale bar represents 1 cm. (b) CD spectra of CNC films under the mask.

and allowed the suspension to completely evaporate before removal of the mask. As shown in Figure 3a, we obtained a red CNC film with blue features, where the mask was placed during the evaporation process. Characterization with CD

DOI: 10.1021/acsanm.8b00947
ACS Appl. Nano Mater. 2018, 1, 3098−3104

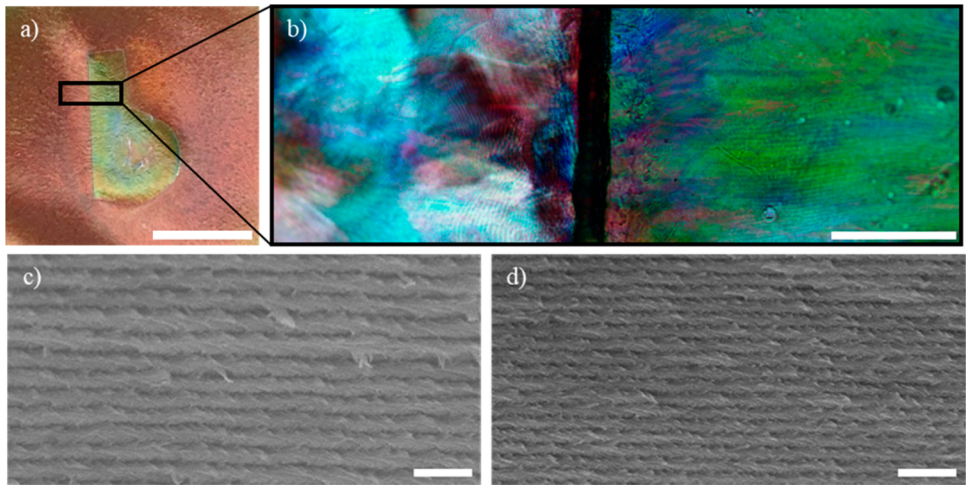

Figure 5. Patterned CNC film prepared with a "b" lettered mask. (a) Photograph of the patterned film. (b) POM image of both the unmasked (left) and masked (right) regions separated by an interface. Cross-sectional SEM images of (c) unmasked and (d) masked regions of the "b" patterned CNC film. The scale bars represent (a) 1 cm, (b) 100 μm, and (c and d) 1 μm.

spectroscopy showed a decrease in the reflection wavelength at regions under the mask (Figure 3b). It should be noted that a small depression exists at the edge of the mask upon removal, likely due to surface tension during the final stages of drying. Thus, spectra were collected at the center of the CNC film to avoid these defect sites. Between the masked and unmasked regions, the chiral nematic structure is maintained, as shown by cross-sectional scanning electron microscopy (SEM; Figure 3c,d).

The colors of the patterns can also be tuned depending on the stage of evaporation at which we place the cellulose acetate masks on the CNC suspension. CNC films were cast, and cellulose masks were placed 0, 6, or 9 h after the CNC suspensions were cast (Figure S4). The resulting films have significantly different optical properties when placed under the masks at different times (Figure 4a).

The cellulose acetate mask increases the evaporation time of the CNC suspension by up to 10 days and results in a blue-shifted reflection wavelength, as confirmed by CD spectroscopy, compared to the unmasked region (Figure 4b). We hypothesize that the stage of self-assembly is very important in determining the resulting film's optical properties. The immediate application of a mask led to the largest difference in the reflection wavelength, from red to blue, whereas the optical properties were nearly unaffected when the mask was applied at a late stage of evaporation, in this case after 9 h (ca. 8 wt % CNCs). It is possible that the stage of self-assembly responsible for the formation of the helical pitch occurs at a point before gel vitrification (ca. 8 wt % CNCs). We demonstrate that the critical aspect of pattern formation is heavily influenced by the evaporation time. Factors that influence the evaporation rate can be used to manipulate the patterns on CNC films. For instance, the use of pressure, light, or heated masks are other interesting ways to influence the rate of evaporation, and it would be interesting to study these types of patterned CNC films in the future.

A closer look at polarized optical microscopy (POM) of the "b" masked film reveals a difference in the domain size between the masked and unmasked regions (Figure 5a,b). This suggests that the overall film order is improved where the mask is applied. Conversely, the "c" masked film does not show this difference in the domain size, which further suggests that structural changes can occur up until gel vitrification locks in the structures (Figure S3).

Helical pitches were measured from SEM images of the cross sections of the films, resulting in half-helical pitches of 411 ± 58 nm (n = 16) and 286 ± 33 nm (n = 16) in the unmasked and masked regions, respectively, which correspond well with the CD spectra (Figures 4b and 5c,d). Overall, we have shown that patterns can be easily produced with the use of masks, resulting in distinct regions under the masked or unmasked regions. This level of control will be important to further study the nuances of the self-assembly process as we make progress toward controlling the optical properties of CNC-based materials.

CONCLUSION

The optical properties of CNC films can be tuned by controlling the evaporation of the CNC suspension. Evaporation under ambient conditions led to red films, whereas slow evaporation resulted in blue-shifted films. Differential evaporation represents an easy approach to the development of patterned CNC films. Furthermore, the use of a mask to restrict the evaporation to well-defined regions also opens up opportunities to study different mask architectures and compositions for the patterning of CNC films. These findings are important for applying our current understanding of the self-assembly in CNC-based systems to develop CNC materials for optical applications.

EXPERIMENTAL SECTION

Materials. All compounds were used as received without any further purification. Aqueous suspensions of CNCs were provided by FPInnovations (CNC-H^+, 4.2 wt %, pH 2.1). In brief, ultrapure aqueous CNC suspensions were prepared by dispersing spray-dried CNCs in deionized water, at a concentration of 2 wt %, by stirring the suspension overnight using a mechanical stirrer.[36] The dispersed CNC suspension was then sonicated at 70% power for 30 min (in batches of 3 L) using a Vibra-Cell VC750 ultrasonicator (Sonics & Materials Inc.). The average energy input was ~9000 J g^{-1} of CNCs. The suspension was then filtered, first using grade 4 Whatman filter paper, followed by grade 42 Whatman filter paper. The filtered CNC suspension was dialyzed against deionized water overnight. The dialyzed suspension was concentrated to the desired concentration using a rotary evaporator and then stored in a refrigerator at 4 °C

DOI: 10.1021/acsanm.8b00947
ACS Appl. Nano Mater. 2018, 1, 3098−3104

until further use. The final pH and conductivity of the ultrapure CNC aqueous suspension were adjusted to acidic form (CNC-H^+, pH 2.1) using an ion-exchange resin (Dowex Marathon C hydrogen form, 23–27 mesh particle size, Sigma-Aldrich). The dimensions of the CNC spindles were determined by transmission electron microscopy size distribution analysis to be 191 ± 80 nm and to have an electrophoretic surface charge of −4.44. All CNC suspensions were sonicated for 1 h prior to use. The control film in each experiment involved the casting of 3.9 mL of CNC suspension in a 50 mm polystyrene Petri dish, followed by evaporation under ambient conditions over a period of ∼1 day. Ambient conditions were 23.6 °C at ∼50% relative humidity.

Evaporation Dependence on CNC Film Formation. CNC suspensions (3.9 mL, 4.2 wt %) were cast in Petri dishes. A suspension was immediately covered with a lid that covered the entire suspension and left to evaporate over 10 days at ∼15 mg h^{-1}. A control film was prepared without a lid and evaporated over 1 day at ∼145 mg h^{-1}.

Patterning of CNC Films with Differential Evaporation. CNC suspensions (3.9 mL, 4.2 wt %) were cast in Petri dishes. A lid containing a circular opening at the center, with a diameter of 1 cm, was placed on top of the CNC suspension. The suspension was left to evaporate until a film formed.

Patterning CNC films with Cellulose Acetate Masks. CNC suspensions (3.9 mL, 4.2 wt %) were cast in Petri dishes. Cellulose acetate masks, cut into either shapes (circles) or letters (U, b, and c), were placed on CNC suspensions either 0, 6, or 9 h after casting. CNC suspensions were left to evaporate until both regions, masked and unmasked, formed films.

Instrumentation. SEM was performed at the UBC Bioimaging Facility on a Hitachi S4700 electron microscope (Hitachi Ltd.). Cross sections of CNC films were prepared by cleanly breaking films between two glass slides and then mounting them on sample holders. Films were then sputter-coated with 8 nm of platinum (99.99%; ρ = 21.45 g cm^{-3}) before imaging. The SEM stage was tilted 90°, and cross-sectional images of CNC films were obtained, typically at 5 kV accelerating voltage and 10 μA current. Light transmittance (% T) and CD spectroscopy of solid CNC films were performed on Cary 5000 UV–vis (Agilent Technologies) and Jasco J-815 (Jasco Inc.) spectrophotometers, respectively, at the UBC Shared Instrument Facility. Films were mounted perpendicular to the incident light source, and spectra were collected over the visible spectrum (350–800 nm) for both UV–vis and CD spectroscopy. The optical properties were measured at θ = 0° incident light, with air as the reference in each experiment. POM images were taken on an Olympus BX41 (Olympus Corp.) optical microscope. Solid films were imaged between two linear polarizers placed at 90° with respect to each other.

■ ASSOCIATED CONTENT

Supporting Information

The Supporting Information is available free of charge on the ACS Publications website at DOI: 10.1021/acsanm.8b00947.

Figures S1–S4 (PDF)

■ AUTHOR INFORMATION

Corresponding Author

*E-mail: mmaclach@chem.ubc.ca.

ORCID

Mark J. MacLachlan: 0000-0002-3546-7132

Author Contributions

The manuscript was written through contributions of all authors. All authors have given approval to the final version of the manuscript.

Notes

The authors declare no competing financial interest.

■ ACKNOWLEDGMENTS

A.T. thanks his parents for support and the University of British Columbia for a 4YF fellowship. M.J.M. thanks NSERC (Discovery, CREATE NanoMat) for support.

■ ABBREVIATIONS

CNC = cellulose nanocrystal
SEM = scanning electron microscopy
CD = circular dichroism
POM = polarized optical microscopy

■ REFERENCES

(1) Habibi, Y.; Lucia, L. A.; Rojas, O. J. Cellulose Nanocrystals: Chemistry, Self-Assembly, and Applications. *Chem. Rev.* **2010**, *110*, 3479–3500.

(2) Araki, J.; Wada, M.; Kuga, S.; Okano, T. Flow Properties of Microcrystalline Cellulose Suspension Prepared by Acid Treatment of Native Cellulose. *Colloids Surf., A* **1998**, *142*, 75–82.

(3) Beck-Candanedo, S.; Roman, M.; Gray, D. G. Effect of Reaction Conditions on the Properties and Behavior of Wood Cellulose Nanocrystal Suspensions. *Biomacromolecules* **2005**, *6*, 1048–1054.

(4) De Souza Lima, M. M.; Wong, J. T.; Paillet, M.; Borsali, R.; Pecora, R. Translational and Rotational Dynamics of Rodlike Cellulose Whiskers. *Langmuir* **2003**, *19*, 24–29.

(5) Roman, M.; Winter, W. T. Effect of Sulphate Groups from Sulphuric Acid Hydrolysis on the Thermal Degradation Behaviour of Bacterial Cellulose. *Biomacromolecules* **2004**, *5*, 1671–1677.

(6) Revol, J. F.; Godbout, L.; Gray, D. G. Solid Self-Assembled Films of Cellulose with Chiral Nematic Order and Optically Variable Properties. *J. Pulp Pap. Sci.* **1998**, *24*, 146–149.

(7) Hiratani, T.; Hamad, W. Y.; MacLachlan, M. J. Transparent Depolarizing Organic and Inorganic Films for Optics and Sensors. *Adv. Mater.* **2017**, *29*, 1606083.

(8) Eichhorn, S. J.; Young, R. J. The Young's Modulus of a Microcrystalline Cellulose. *Cellulose* **2001**, *8*, 197–207.

(9) Ureña-Benavides, E. E.; Ao, G.; Davis, V. A.; Kitchens, C. L. Rheology and Phase Behavior of Lyotropic Cellulose Nanocrystal Suspensions. *Macromolecules* **2011**, *44*, 8990–8998.

(10) Klemm, D.; Kramer, F.; Moritz, S.; Lindström, T.; Ankerfors, M.; Gray, D.; Dorris, A. Nanocelluloses: A New Family of Nature-Based Materials. *Angew. Chem., Int. Ed.* **2011**, *50*, 5438–5466.

(11) Siqueira, G.; Kokkinis, D.; Libanori, R.; Hausmann, M. K.; Gladman, A. S.; Neels, A.; Tingaut, P.; Zimmermann, T.; Lewis, J. A.; Studart, A. R. Cellulose Nanocrystal Inks for 3D Printing of Textured Cellular Architectures. *Adv. Funct. Mater.* **2017**, *27*, 1604619.

(12) Markstedt, K.; Mantas, A.; Tournier, I.; Martínez Ávila, H.; Hägg, D.; Gatenholm, P. 3D Bioprinting Human Chondrocytes with Nanocellulose-Alginate Bioink for Cartilage Tissue Engineering Applications. *Biomacromolecules* **2015**, *16*, 1489–1496.

(13) Lagerwall, J. P. F.; Schutz, C.; Salajkova, M.; Noh, J.; Hyun Park, J.; Scalia, G.; Bergström, L. Cellulose Nanocrystal-Based Materials: From Liquid Crystal Self-Assembly and Glass Formation to Multifunctional Thin Films. *NPG Asia Mater.* **2014**, *6*, e80.

(14) Gray, D. G. Recent Advances in Chiral Nematic Structure and Iridescent Color of Cellulose Nanocrystal Films. *Nanomaterials* **2016**, *6*, 213–221.

(15) Parker, R. M.; Guidetti, G.; Williams, C. A.; Zhao, T.; Narkevicius, A.; Vignolini, S.; Frka-Petesic, B. The Self-Assembly of Cellulose Nanocrystals: Hierarchical Design of Visual Appearance. *Adv. Mater.* **2017**, *1704477*.

(16) Rånby, B. G. The Colloidal Properties of Cellulose Micelles. *Discuss. Faraday Soc.* **1951**, *11*, 158–164.

(17) Hamad, W. Y. Development and Properties of Nanocrystalline Cellulose. In *Sustainable production of fuels, chemicals, and fibers from forest biomass*;Zhu, J. Y., Zhang, X., Pan, X.,, Eds.; American Chemical Society: Washington, DC, 2011; pp 301–321.

DOI: 10.1021/acsanm.8b00947
ACS Appl. Nano Mater. 2018, 1, 3098–3104

(18) Revol, J. F.; Bradford, H.; Giasson, J.; Marchessault, R. H.; Gray, D. G. Helicoidal Self-Ordering of Cellulose Microfibrils in Aqueous Suspension. *Int. J. Biol. Macromol.* **1992**, *14*, 170−172.
(19) Wang, P.-X.; Hamad, W. Y.; MacLachlan, M. J. Structure and Transformation of Tactoids in Cellulose Nanocrystal Suspensions. *Nat. Commun.* **2016**, *7*, 11515.
(20) De Vries, H. L. Rotatory Power and Other Optical Properties of Certain Liquid Crystals. *Acta Crystallogr.* **1951**, *4*, 219−226.
(21) Vukusic, P.; Sambles, J. R.; Lawrence, C. R.; Wootton, R. J. Quantified Interference and Diffraction in Single Morpho Butterfly Scales. *Proc. R. Soc. London, Ser. B* **1999**, *266*, 1403−1411.
(22) Crookes, W. J.; Ding, L.; Huang, Q. L.; Kimbell, J. R.; Horwitz, J.; McFall-Gnai, M. J. Reflectins: The Unusual Proteins of Squid Reflective Tissues. *Science (Washington, DC, U. S.)* **2004**, *303*, 235−238.
(23) Sharma, V.; Crne, M.; Park, J. O.; Srinivasarao, M. Structural Origin of Circularly Polarized Iridescence in Jeweled Beetles. *Science (Washington, DC, U. S.)* **2009**, *325*, 449−451.
(24) Vignolini, S.; Rudall, P. J.; Rowland, A. V.; Reed, A.; Moyroud, E.; Faden, R. B.; Baumberg, J. J.; Glover, B. J.; Steiner, U. Pointillist Structural Color in Pollia Fruit. *Proc. Natl. Acad. Sci. U. S. A.* **2012**, *109*, 15712−15715.
(25) Mu, X.; Gray, D. G. Formation of Chiral Nematic Films from Cellulose Nanocrystal Suspensions Is a Two-Stage Process. *Langmuir* **2014**, *30*, 9256−9260.
(26) Pan, J.; Hamad, W.; Straus, S. K. Parameters Affecting the Chiral Nematic Phase of Nanocrystalline Cellulose Films. *Macromolecules* **2010**, *43*, 3851−3858.
(27) Dumanli, A. G.; Kamita, G.; Landman, J.; van der Kooij, H.; Glover, B. J.; Baumberg, J. J.; Steiner, U.; Vignolini, S. Controlled, Bio-Inspired Self-Assembly of Cellulose-Based Chiral Reflectors. *Adv. Opt. Mater.* **2014**, *2*, 646−650.
(28) Natarajan, B.; Emiroglu, C.; Obrzut, J.; Fox, D. M.; Pazmino, B.; Douglas, J. F.; Gilman, W. Dielectric Characterization of Confined Water in Chiral Cellulose Nanocrystal Films. *ACS Appl. Mater. Interfaces* **2017**, *9*, 14222−14231.
(29) Frka-Petesic, B.; Guidetti, G.; Kamita, G.; Vignolini, S. Controlling the Photonic Properties of Cholesteric Cellulose Nanocrystal Films with Magnets. *Adv. Mater.* **2017**, *29*, 1701469.
(30) Frka-petesic, B.; Radavidson, H.; Jean, B.; Heux, L. Dynamically Controlled Iridescence of Cholesteric Cellulose Nanocrystal Suspensions Using Electric Fields. *Adv. Mater.* **2017**, *29*, 1606208.
(31) Nguyen, T.-D.; Hamad, W. Y.; MacLachlan, M. J. Tuning the Iridescence of Chiral Nematic Cellulose Nanocrystals and Mesoporous Silica Films by Substrate Variation. *Chem. Commun.* **2013**, *49*, 11296−11298.
(32) Dong, X. M.; Kimura, T.; Revol, J.-F.; Gray, D. G. Effects of Ionic Strength on the Isotropic−Chiral Nematic Phase Transition of Suspensions of Cellulose Crystallites. *Langmuir* **1996**, *12*, 2076−2082.
(33) Tran, A.; Hamad, W. Y.; MacLachlan, M. J. Tactoid Annealing Improves Order in Self-Assembled Cellulose Nanocrystal Films with Chiral Nematic Structures. *Langmuir* **2018**, *34*, 646−652.
(34) Beck, S.; Bouchard, J.; Chauve, G.; Berry, R. Controlled Production of Patterns in Iridescent Solid Films of Cellulose Nanocrystals. *Cellulose* **2013**, *20*, 1401−1411.
(35) Harris, D. J.; Hu, H.; Conrad, J. C.; Lewis, J. A. Patterning Colloidal Films via Evaporative Lithography. *Phys. Rev. Lett.* **2007**, *98*, 148301.
(36) Hamad, W. Y.; Hu, T. Q. Structure-Process-Yield Interrelations In Nanocrystalline Cellulose Extraction. *Can. J. Chem. Eng.* **2010**, *88*, 392−402.

DOI: 10.1021/acsanm.8b00947
ACS Appl. Nano Mater. 2018, 1, 3098−3104